Nickel Phosphide Catalyst for Autothermal Reforming of Surrogate Gasoline Fuel

Lei Liu and Liang Hong
Dept. of Chemical and Biomolecular Engineering, National University of Singapore, Singapore 117576

DOI 10.1002/aic.12505
Published online February 8, 2011 in Wiley Online Library (wileyonlinelibrary.com).

An investigation into the catalytic autothermal reforming (ATR) of a mixture of n-*octane and naphthalene (6 wt %), designed as a surrogate gasoline, is undertaken. Carbon deposition on the metallic Ni catalyst has been aware of the main hurdle for the catalytic reforming of hydrocarbons especially those with high carbon numbers. This work develops Ni_xP_y crystallites on a CeO_2 powder support by electroless nickel plating and calcination. The catalyst exhibits nil coking extent after reforming the surrogate fuel. The Ni_xP_y crystallites are determined by XRD and its Ni-P bonding is confirmed by XPS, where the Ni carries slightly higher negative charge than the Ni^0 as usually observed. The XPS investigation also divulges the presence of Ce^{3+} species in the CeO_2 support on which the Ni_xP_y crystallites are distributed, indicating that the support contains oxygen vacancies. These two subtle structural differences are proposed to provide the catalyst with resistance to coking.* © 2011 American Institute of Chemical Engineers *AIChE J,* 57: 3143–3152, 2011
Keywords: autothermal reforming, coking, electroless plating, supported-ni catalyst, liquid hydrocarbons

Introduction

Fuel cells powered by hydrogen or syngas (H_2/CO) possess advantages of high energy efficiency and clean emission over internal combustion engines. Conducting reforming of gasoline or diesel whose main component comprises C_4 to C_{16} hydrocarbons for the production of hydrogen on board is of special interest. This route could avoid shipping and storage of hydrogen or syngas and allow for continuous use of the existing fossil oil delivery infrastructure.[1,2] Hence, development of a Ni-based catalyst possessing adequate chemical stability in the reforming of larger molecular weight hydrocarbons, such as gasoline or diesel, is crucial to the evolution of this clean energy source. Regarding the existing catalytic reforming techniques, that is, steam reforming (SR) and partial oxidation (POX), and their combination generates autothermal reforming (ATR). As a result, the exothermic POX could cover the heat the endothermic SR reaction demands.[3] A typical ATR is (taking *n*-octane for example):

$$C_8H_{18} + xO_2 + (16 - 2x)H_2O \underset{\text{cat}}{\rightarrow} 8CO_2 + (25 - 2x)H_2 \quad (1)$$

where x is the oxygen-to-fuel molar ratio. The degree of the exothermic (POX) or the endothermic (SR) of the overall reaction can be controlled by the x value.

The chemical stability of the Ni-based catalyst is about its capability to avert the deactivating actions of sulfur-containing compounds and coke deposited. Deposition of carbon at Ni catalyst during the reforming of hydrocarbons is a hazard to POX and ATR because coking causes jam in a packed-bed reactor and deactivation of catalyst.[4] The mechanism of carbon deposition at the Ni catalyst has been extensively investigated.[5,6] Nevertheless, most of them focused on the POX of methane in which impregnated Ni catalysts were used. Furthermore, compared with methane, it would be more difficult to reform liquid hydrocarbons due to a heavier coke deposition extent. To tackle this problem, the precious metal-modified Ni catalysts and the supported-precious metal catalysts have been

Correspondence concerning this article should be addressed to L. Hong at chehongl@nus.edu.sg.

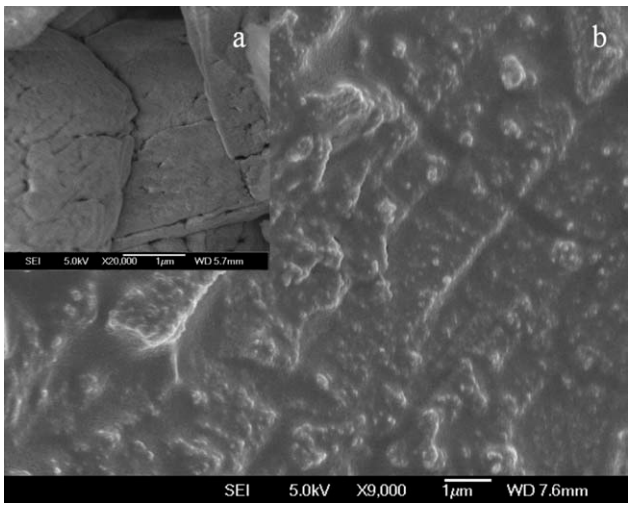

Figure 1. FE-SEM images of the surface morphology of the ceria particles adopted as support (a) and that of the modified ceria particles (b).

explored to reform long-chain alkanes under the autothermal condition.[7–11] Despite displaying stronger resistance to carbon deposition than nickel, noble metals are in general too costly to suit industrial applications. Hence, the supported-Ni catalyst system still remains practically attractive. Modification of the refractory oxides supports has been an effective way to improve coking resistance at the Ni crystallites supported on them. Recently, the doped cerium oxides have become a novel type of support mainly because they contain oxygen vacancies. Lattice oxygen ions in the doped ceria could contribute to removing of carbon filaments from the Ni catalyst at the reforming temperatures.[12–15]

Different from using the impregnated Ni catalyst, we synthesized nano-sized NiP alloy nodules on micronsized particles of ceria by means of the electroless nickel plating (ENP). Despite being an amorphous alloy, the as-deposited Ni(P) (P $\sim$ 12 wt %) nodules were converted to nickel phosphide crystallites, Ni_xP_y, at the reaction temperature of ATR. In the following sections we denote the CeO_2-supported Ni_xP_y catalyst as NiP/Ce for the sake of simplicity. In principle, the nickel phosphide crystallite is formed by polar covalent bonding. It has been reported recently that the Ni_xP_y catalyst, obtained from a different ENP procedure, was used to catalyze dechlorination of an organic chloride.[16] This work focuses on understanding how the designated catalytic conditions affect the conversion of the surrogate hydrocarbon fuel and the yields of H_2, CO, CO_2, and CH_4. It has been also confirmed that the NiP/Ce catalyst remained carbon-free after the ATR of the fuel consisting of *n*-octane and naphthalene. Fundamental aspects for this improvement have also been explored experimentally.

Experimental

Preparation of the catalyst precursor Ni(P)/Ce and a control catalyst

The catalyst was initially prepared by depositing Ni(P) nano nodules to ceria particles (CeO_2, <5 μm, 99.9%, Sigma Aldrich) in an acidic electroless nickel plating bath.[17] Before plating, the ceria particles were modified by the following surface roughening procedure. First, 5 g ceria was added into 100 ml solution of cerium hexahydrate [$Ce(NO)_3{\cdot}6H_2O$, 2.52 g] under stirring. The pH value of the slurry formulated was adjusted to about 10.0 by dropping 2.5% ammonia solution into the slurry. The slurry was then stirred for 1 h and aged subsequently for 4 h. During this treatment, most of $Ce(OH)_4$ precipitate first attached to the CeO_2 particles and then formed a gel layer. The solid was collected by filtration, followed by drying overnight at 80°C and calcining at 600°C for 1 h. This step enhanced the surface roughness, which was confirmed by both the increase in specific surface area from 7 to 17 $m^2\ g^{-1}$ and micrograph image of the CeO_2 particles (Figure 1). The modified oxide powder was then sensitized in an aqueous solution containing stannous chloride ($SnCl_2{\cdot}2H_2O$, 20 g L^{-1}) and hydrochloric acid (0.24 M) under stirring for 10 min at room temperature. The sensitized oxide was rinsed with deionized (DI) water subsequently. Then the oxide was activated in an aqueous solution containing palladium chloride ($PdCl_2{\cdot}2H_2O$, 0.3 g L^{-1}) and hydrochloric acid (0.12 M) under stirring for 5 min at room temperature. After that, the oxide was fully washed using DI water and dried at 50°C in vacuum. A certain amount of the activated ceria was transferred into the nickel plating solution with pH = 5 and 60°C for 10 min with constant stirring. The recipe of the nickel plating solution is listed in Table 1. After plating, the powder was washed thoroughly with DI water and dried at 50°C in vacuum. After that, the Ni(P) deposited ceria, Ni(P)/Ce, obtained has a Ni loading of 5.6 wt % and a ratio of Ni to P by weight of about 7. Finally it is worthy of note that such extent of plating cannot be attained without enhancing surface roughness of CeO_2 particles.

One of the two control catalysts used in this study was prepared by the impregnation method as reported everywhere. An appropriate amount of $Ni(NO_3){\cdot}6H_2O$ was dissolved in 50-ml DI water, then the ceria powder was added into this solution. After stirring under room temperature for about 3 h, the mixture was heated at 60°C overnight under stirring to evaporate water. The obtained solid was calcined in air at 600°C for 3 h to obtain a NiO/Ce powder. It would be then reduced to Ni/Ce under ATR conditions. The Ni loading in this control catalyst was about the same as the Ni(P)/Ce. Finally, a nickel-based SR commercial catalyst (HiFUEL, Ni loading: 15–40 wt % denoted by CC) was adopted as another control catalyst to benchmark the performance of the NiP/Ce catalyst.

Characterizations of catalyst

The composition of the catalyst precursor Ni(P)/Ce was determined by Inductively Coupled Plasma-Mass Spectrometry (ICP-MS, Agilent 7500 Series). The total nickel loading was about 5.6 wt %, whereas the Ni(P) alloy comprised 87.5

Table 1. Compositions of Electroless Nickel Plating Bath

Chemical	Concentration
Nickel nitrate hexahydrate	22.4 g L^{-1}
Sodium hypophosphite	25 g L^{-1}
DL-malic acid	4 g L^{-1}
Sodium acetate	8.5 g L^{-1}
Lactic acid	21 ml L^{-1}
Borax	6 g L^{-1}
Lead acetate	3 mg L^{-1}

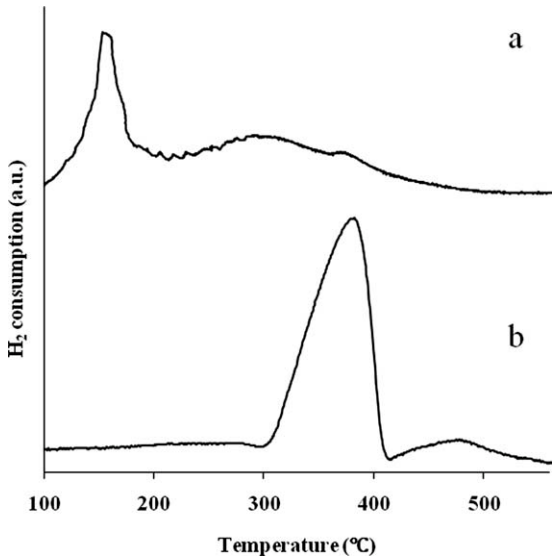

Figure 2. TPR profiles of (a) fresh Ni(P)/Ce and (b) NiO/Ce.

wt % of Ni and 12.5 wt % of P. The content of palladium is about 0.3 wt %. The specific surface area of the precursor was gauged on an Autosorb-1 (Quantachrome) by applying the multipoint BET method after degassing at 300°C for 3 h under N_2 purging. Its magnitude is about $30 m^2\ g^{-1}$. The temperature-programmed reduction (TPR) was conducted on the same instrument using a sample of 100 mg and a gas (5% H_2 in N_2) flow rate of 80 ml min^{-1}. The heating rate was set as 10°C min^{-1}. The morphologies of the different catalysts were observed and recorded on a field-emission scanning electron spectroscope instrument (JEOL, JSM-6700F). Crystalline structures of the catalysts were determined on an X-ray diffractometer (XRD, SHIMADZU XRD-6000, Cu Kα radiation) using a scanning rate of 5° min^{-1}. The oxidation states of Ni, P and Ce in the NiP/Ce and Ni/Ce catalysts were characterized on an instrument of X-ray photoelectron spectroscopy (XPS, Kratos Axis HiS System) equipped with Al *K*α X-ray source (1486.6 eV) and the take-off angle of 90° with pass energy of 40 eV. C1s (284.6 eV) was used as the internal reference to calibrate the spectra obtained. To double confirm the carbon filament deposited on the Ni/Ce catalyst but not on the NiP/Ce catalyst during ATR of the *n*-octane, two temperature-programmed oxidation profiles of the two catalysts were obtained respectively from the measurement on a (Quantachrome ChemBET 3000). Typically, ca. 50 mg sample was placed in a U-tube holder and subsequently degassed at 300°C for 1 h by flushing the sample with N_2 gas at a flow rate of 80 ml/min. After degassing, the probe gas consisting of 5% O_2 and N_2 was allowed to pass through the sample at a flow rate of 55 ml/min, and then the sample was heated from ambient temperature to 1000°C, over which a TPO profile was recorded.

Experimental setup and reaction conditions

Approximately, 1 g catalyst powder was packed between two plugs of quartz wool in the center of a quartz tube reactor (1.2 cm o.d., 1 cm i.d., 40 cm long). The micro plug flow reactor was then placed in a thermostat-controlled vertical tube furnace. The air and nitrogen mixture into the reactor was metered by Alicat mass flow controller. The fuel (*n*-octane or *n*-octane containing 6 wt % naphthalene) and water streams were regulated respectively by ISO-2000 isocratic pumps and sent to joining with the air/N_2 stream. The tri-components (fuel, air/N_2 and water) stream was then directed into a mixer wrapped up by a heating band to carry out vaporization and mixing before being connected to the catalytic bed. The temperature of the mixer was set at 250°C and a blank run indicated that the fuel was not pyrolyzed in the mixer. Before the reaction starts, the catalyst was exposed to a flow of air (30 ml min^{-1}) for about 30 min at 900°C to convert the amorphous Ni(P) alloy to Ni_xP_y crystallite (or NiP as denoted). The optimal reforming conditions comprised the following parameters: fuel-supply rate = 0.04 ml min^{-1}, oxygen and steam supply rates: $O_2/C = 0.5$ and $H_2O/C = 1.7$, reforming temperature 900°C, and GHSV = 9000 ml h^{-1} g_{cat}^{-1}. It may be noted that although identical amounts of the CC catalyst and the Ni(P)/Ce catalyst were loaded to satisfy the same GHSV, the former one contained a higher Ni content by several times. The outlet stream was connected to a Shimadzu GC after passing a cold trap to knock out any condensable components. The performance of the catalyst was assessed by fuel conversion, distribution of gaseous products and their yields, which were evaluated using the following equations where nitrogen was used as internal standard:

$$\text{Conversion} = \frac{F_{total}(y_{CO} + y_{CO_2} + y_{CH_4})}{F_C \text{ in fuel}} \quad (2)$$

$$\text{Yield} = \frac{F_{total}\ y_p}{F_p \text{ in fuel}} \quad (3)$$

$$F_{total} = \frac{F_{N_2} \text{ in feed}}{y_{N_2}} \quad (4)$$

where F stands for molar flow rate in mol s^{-1} and y the mole fraction of a component *p* (subscript) in the gas outlet stream. F_p stands for the mass flow rate of component p in the feed (for hydrogen, H_2 is used as the basic unit for calculation). Theoretically the conversion should be determined from the amount of octane at the exit of the reactor with respect to that used in the feed. However, the fuel conversion is determined using Eq. 2 here due to some practical reasons, such as limitation of gas analysis and the removal of fuel in the water condensation process.

Results and Discussion

Determination of the ATR conditions

Prepared by the electroless plating, the amorphous Ni(P)/Ce displays a complete different TPR profile from the NiO/Ce prepared by the impregnation method (Figure 2). The TPR diagram of Ni(P)/Ce presents only a sharp peak at 150°C and a broad peak centred at 290°C with a shoulder peak at 363°C, while NiO/Ce revealed the normal exothermic reduction peak of NiO at about 380°C. The sharp peak at 150°C represents reduction of superficial passivation layer on the Ni(P) nodules. The broad peak at 290°C can be

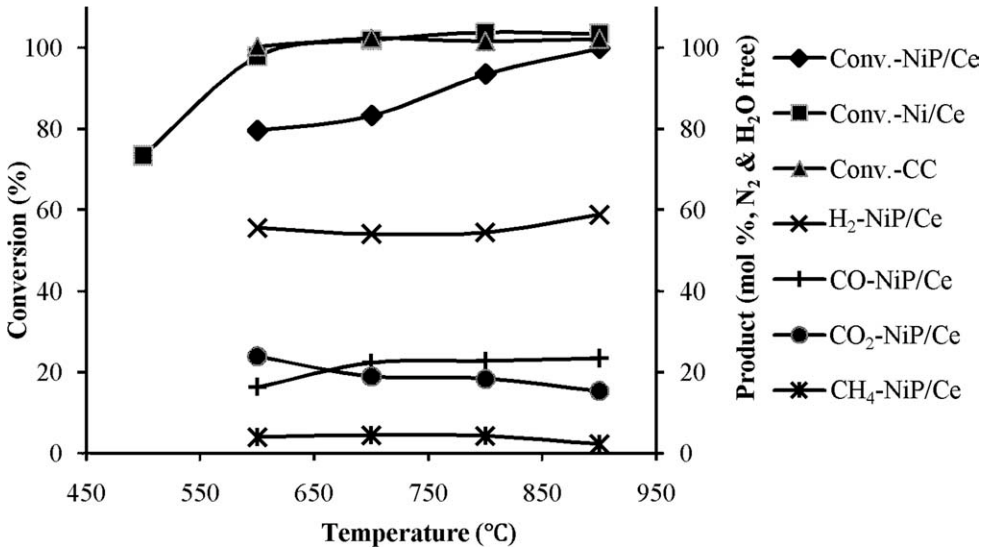

Figure 3. Variation of *n*-octane conversions (wrt. the three catalysts) and the concentrations of the four species in the product stream (from the NiP/Ce system) with reaction temperature (C_8H_{18} = 0.04 ml min^{-1}, O_2/C = 0.5, H_2O/C = 1.7, GHSV = 9000 ml h^{-1} g_{cat}^{-1}).

ascribed to the reduction of Ce^{4+} ions of the ceria support by referencing the reported work,[18] whereas the broad peak at 480°C on the TPR of the NiO/Ce catalyst is known to be the normal reduction peak of ceria. As can be found, the two ceria supports exhibit discrepant reduction temperatures and peak intensities, namely, the reducibility, just because of the presence of the two different catalysts on them. According to the previous studies,[18,19] the supported noble metal catalysts (Pt, Rh) reveal unique capability to facilitate reduction of the ceria support underneath. This facilitation leads to generation of oxygen vacancies in ceria and thus enhances the oxygen conductivity of the support, helping clean up in-situ carbon filaments formed during the reforming reaction.

The conversion of *n*-octane (to CH_4, CO, and CO_2) increases with the increase in temperature (Figure 3). However, the concentration of H_2 is basically not affected by reaction temperature while the concentration of CO slightly increased. Compared with the two control catalysts, viz. CC and Ni/Ce, NiP/Ce shows lower conversions at temperatures below 900°C but finally presents a comparable activity at 900°C. Therefore, the subsequent investigations were undertaken at this temperature.

As indicated in Eq. 1, the O_2/C ratio affects the extents of SR and POX, the sign of reaction heat and the concentration of H_2 in the product stream. The effect of O_2/C ratio on the composition of the product stream is reflected in Figure 4, where the conversion of *n*-octane is independent of the O_2/C ratios. With the increase in O_2/C ratio, the H_2/CO ratio decreases due to an increase in the production of CO. To approximately estimate the O_2/C ratio that leads to the

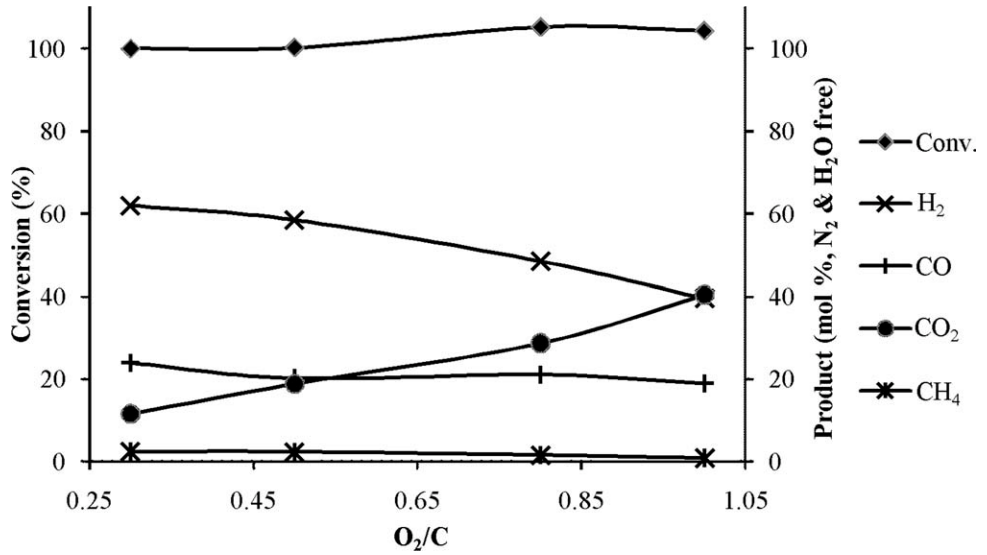

Figure 4. Variation of *n*-octane conversion and the composition of product stream with O_2/C ratio in the NiP/Ce catalytic system (C_8H_{18} = 0.04 ml min^{-1}, H_2O/C = 1.7, 900°C, and GHSV = 9000 ml h^{-1} g_{cat}^{-1}).

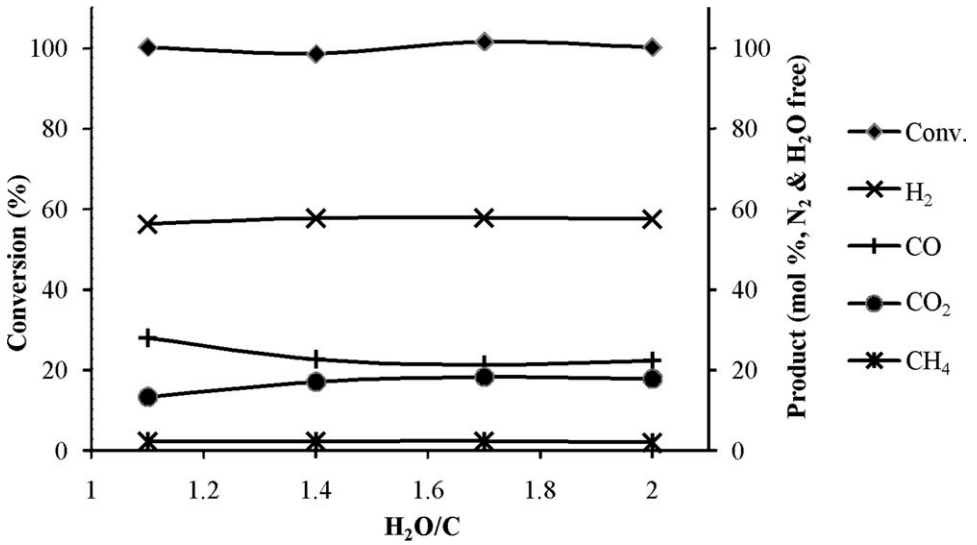

Figure 5. Conversion and composition of the gas product as a function of H_2O/C ratio (C_8H_{18} = 0.04 ml min^{-1}, O_2/C = 0.5, 900°C, GHSV = 9000 ml h^{-1} g_{cat}^{-1}).

thermal balance between POX and SR and results in thermoneutrality of the reaction, the reaction heat at 298 K and the standard state, i.e., $\Delta H^0_{r,298} = 1674.8 - 571.6x$ ($0 \leq x \leq 8$), is used, which is acceptable because enthalpy is a state function. The overall reaction shifts to exothermic direction with the increase in the x value. As a result, when x equals 2.93, namely the O_2/C ratio is about 0.37, the reaction reaches thermoneutral $\Delta H^0_{r,298} = 0$. An O_2/C ratio slightly above 0.37 is desirable to assure the reaction be weak exothermic so that the decrease in H_2% can be minimized. Based on this consideration, the O_2/C ratio of 0.5 was selected to undertake the rest studies. With this ratio, the concentrations of H_2 and CO in the product stream are 60 and 20 mol %, respectively (Figure 4). In addition, the conversion became slightly above 100% with use of the high O_2/C ratios, which is likely due to the effect of cleaning the carbonaceous residues in the mixer prior to reactor.

With respect to the effect of H_2O/C ratio on the product composition, the H_2O/C ratio of 1 was figured out on the basis of the O_2/C ratio of 0.5 (or $x = 4$ in Eq. 1). We also notice that an increase in the H_2O/C ratio from 1.1 to 1.4 brings about a slight increase in the concentrations of H_2 and CO_2 and a decrease in CO in the outlet stream (Figure 5). This variation marks a minor extent of water gas shift reaction (WGSR, $CO + H_2O \rightarrow CO_2 + H_2$). After that, no further shift toward the CO_2 and H_2 side was observed with the increase in H_2O/C ratio. Such a weak degree of WGSR could be due to the exothermic nature of the reaction when the equilibrium is reached at 900°C.

Table 2. Average Conversions of the Three Catalytic Systems During 8 h ATR of *n*-octane and *n*-octane with Naphthalene

	ATR of *n*-octane		ATR of *n*-octane with Naphthalene (6 wt %)	
Catalyst	Average Conversion (%)	Error (%)	Average Conversion	Error (%)
NiP/Ce	98	±2	98	±3
Ni/Ce	98	±3	98	±3
CC	99	±3	98	±2

Evaluation of the catalysts in ATR of n-octane

The three catalysts all manifest a conversion of near 100% (Table 2) under the conditions of $O_2/C = 0.5$, $H_2O/C = 1$ and 900°C. The yields of CO and CO_2 are similar in these three catalysts (Figure 6), while the yield of H_2 produced from the NiP/Ce catalytic system is slightly lower than those from the other two catalytic systems. The yields of H_2 in the three systems are above 1, which suggests the occurring of SR under the reaction conditions adopted. It can also be noted that there is still 2% methane in the product stream from the NiP/Ce catalytic system over the entire evaluation process. This can be attributed to a feeble deactivating effect of phosphorous atoms in the nickel phosphide cluster.

The Ni(P) nodules, deposited by electroless plating on the ceria support, do not display a XRD pattern due to their

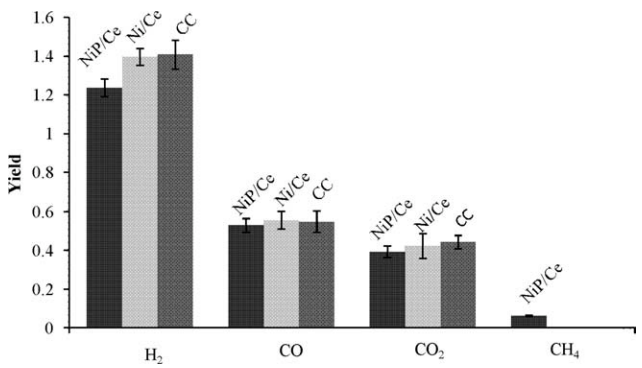

Figure 6. Comparison of the average product yields during 8-h ATR of *n*-octane in the three catalytic systems (C_8H_{18} = 0.04 ml min^{-1}, O_2/C = 0.5, H_2O/C = 1.7, 900°C, GHSV = 9000 ml h^{-1} g_{cat}^{-1}).

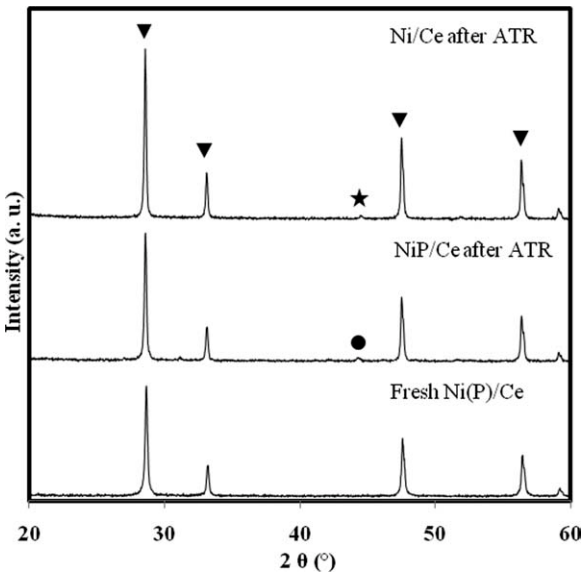

Figure 7. XRD patterns of NiP/Ce before and after ATR, Ni/Ce after ATR. ((▼) CeO2, (●) NiP, (★) Ni).

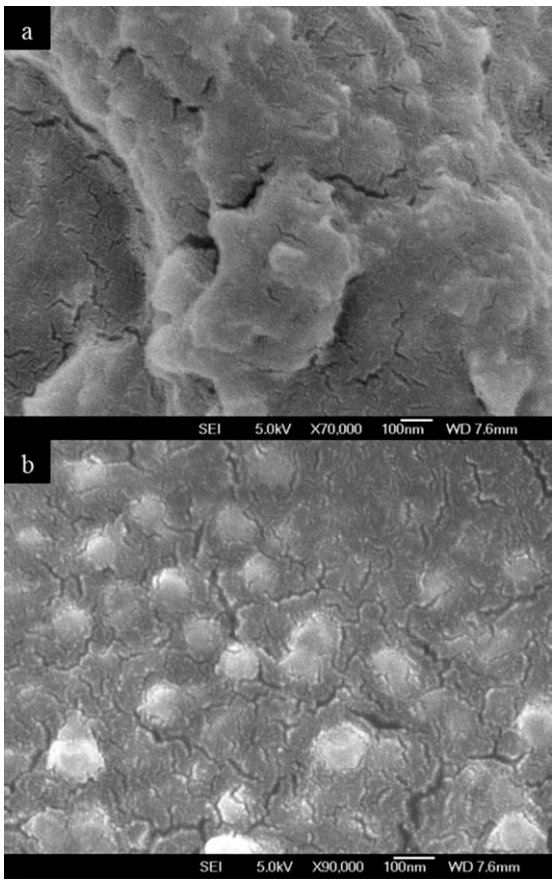

Figure 8. FE-SEM images of (a) the Ni(P)/Ce as electroless deposited and (b) the NiP/Ce after 8-h ATR of *n*-octane.

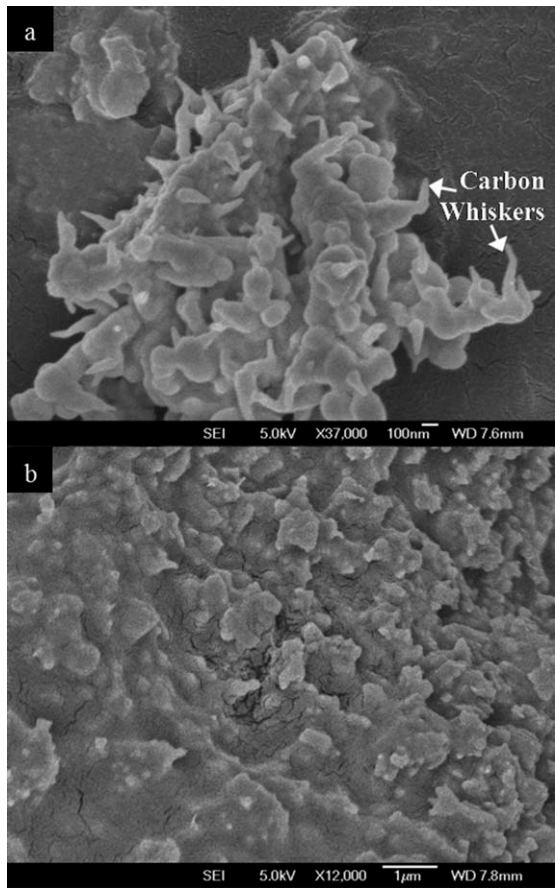

Figure 9. FE-SEM images of the used catalysts: (a) Ni/Ce and (b) CC after 8-h ATR of *n*-octane as shown in Figure 5.

amorphous identity. Nevertheless, the true catalyst is the crystalline NiP cluster, which is generated from the Ni(P) under the ATR conditions. This can be proved by the XRD diagram of the used catalyst (Figure 7). A peak at 44.2° is present on the background of CeO_2 pattern (28.6, 33.1, 47.5, and 56.4°).[19] This peak is the strongest one in the XRD pattern of NiP.[20] As for the Ni/Ce catalyst downloaded from the micro reactor, a small peak at 44.5 ° for Ni (111) is found as expected.[21] On the contrary, the amorphous Ni(P) deposit is converted to crystalline NiP grains (∼ 100 nm) with clear periphery after 8 h ATR (Figure 8). These NiP grains are also confirmed by EDX. It is worthy of note that there were nil carbon filaments grown on the NiP/Ce catalyst after 8 h ATR. On the contrary, short carbon whiskers are found on Ni/Ce catalyst after it is used for ATR under the same conditions (Figure 9). The above identification of carbon filaments is further checked by TPO (Figure 10). A small oxygen uptake peak arises at about 413°C on the TPO profile of Ni/Ce catalyst, which can be assigned to the oxidation of carbon. A similar test based on less sensitive thermogravimetric analysis has reported that carbon oxidation takes place at 665 K.[22] In contrast to this, the used NiP/Ce catalyst does not show such a TPO peak at the temperature nearby but rather a very weak peak at 303°C, which is known to be due to oxidation of a part of Ni on the NiP/Ce catalyst according to XPS study. Similarly, Ni/Ce catalyst

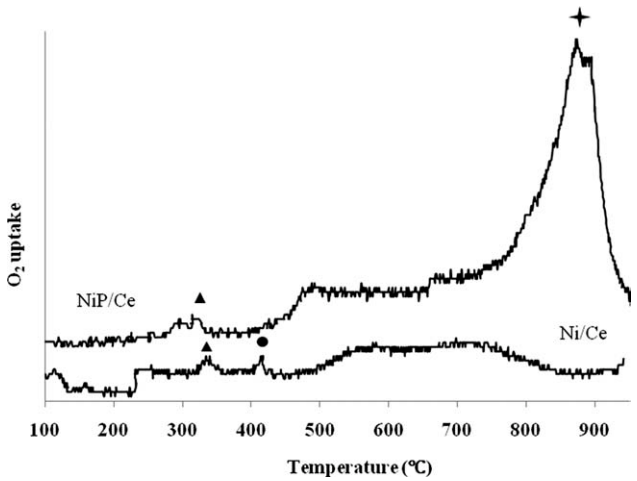

Figure 10. TPO profiles of NiP/Ce and Ni/Ce after 8-h ATR of *n*-octane.

shows a relatively apparent Ni oxidation peak at 330°C. The CC catalyst after ATR is also scrutinized by FE-SEM and it demonstrates better carbon deposition resistance than the Ni/Ce catalyst.

To understand how the P component affects the charge density at Ni before and after ATR, XPS spectra of Ni 2*p* and P 2*p* of the catalyst are investigated (Figure 11). The precursor of catalyst, Ni(P)/Ce, shows the Ni 2*p* doublet: ($2p_{3/2}$) peaks at 855.0 and 852.6 eV. The former peak is the characteristic peak of Ni^{2+} species, whereas the latter is the characteristic peak of Ni^0 species. Similarly, the P 2*p* spectrum could be described by the 2*p* doublet: ($2p_{3/2}$) peaks at 133.0 and 129.3 eV. The former peak can be assigned to P^{5+} of PO_4^{3-} ions, which are the counterion of Ni^{2+}, presumably due to the presence of the $Ni_3(PO_4)_2$ superficial passivation layer that is left behind by the electroless nickel plating.[23,24] On the other hand, the $2p_{3/2}$ component at 129.3 eV characterizes P^0 in the Ni(P) amorphous phase[25–27] where the Ni^0 species has been identified by Ni ($2p_{3/2}$) at 852.6 eV.

After ATR of *n*-octane at 900°C for 8 h, a new peak at 853.6 eV is found in the Ni $2p_{3/2}$ spectrum. It reflects a Ni species carrying the charge between +2 (855.0 eV) and 0 (852.6 eV) as found above. This Ni species is likely those Ni atoms on NiP crystallites that are partially oxidized. It also deserves to note that the Ni^0 ($2p_{3/2}$) component shifts down by about 0.7 to 851.9 eV, which is apparently below the range the reported binding energy of Ni^0 (852.5–852.9 eV).[28] Correspondingly, the P^0 ($2p_{3/2}$) shifts up by about 0.3 to 129.6 eV. This result proposes that the P-Ni bonding in the nickel phosphide cause a slight increase in the electron density at the Ni atom and a slight decrease in electron density at the P atom. It is known that carbon deposition at Ni atoms takes place through thermal cracking of hydrocarbon species. The pristine Ni^0 atomic sites provide suitable Lewis acidity to accept carbon species, leading to the growth of carbon filaments. A slight increase in the electron density at Ni^0 could weaken Lewis acidity of Ni^0.

As far as the effect of ceria support is concerned, we examine the Ce XPS 3*d* spectrum of the used NiP/Ce catalyst (Figure 12). The peaks between 875–895 eV correspond to Ce $3d_{5/2}$, between 895–910 eV correspond to Ce $3d_{3/2}$ and the peak at 916 eV is the characteristic satellite peak corresponding to + 4 states.[29] The peak of Ce^{4+} ions at 888.2 eV displayed by the catalyst precursor shifts to 884.9 eV, known as the characteristic peak of Ce^{3+}.[29] This reduction in the valence of Ce induces generation of oxygen vacancies in the ceria support to maintain the electrical neutrality in its lattice. Namely, the support is converted to O^{2-}conducting phase from CeO_2. Besides the NiP/Ce catalyst, the oxidation states of Ce in the Ni/Ce catalyst and in a particular control catalyst as well, prepared as an activated ceria, are also checked. This control catalyst is prepared by soaking the ceria, obtained from the sensitization and activation treatment, in the electroless plating solution without nickel nitrate under the same ENP conditions (temperature and treatment duration) as used to make Ni(P)/Ce. In contrast to the NiP/Ce catalyst, none of Ce^{3+} species is present in the used Ni/Ce catalyst recovered from ATR under the same condition according to its Ce XPS 3*d* spectrum. Xu and coworkers[30] reported that $CePO_4$ is formed in the automotive exhaust catalyst through the reaction of ceria with gaseous H_3PO_4 and

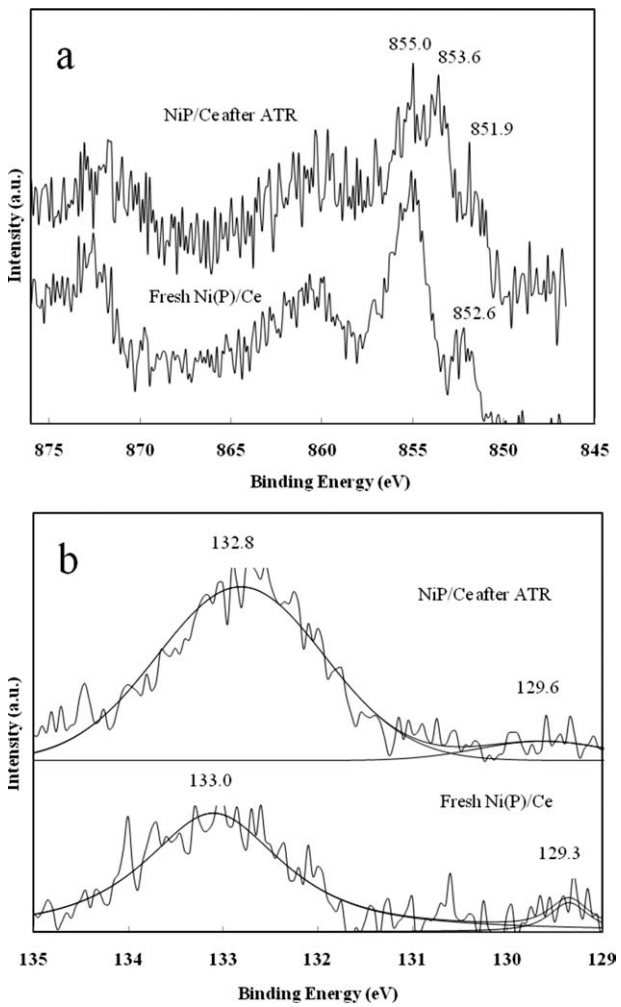

Figure 11. (a) The Ni XPS 2*p* core level spectra and (b) the P XPS 2*p* core level spectra of the NiP/Ce catalyst before and after 8-h ATR respectively.

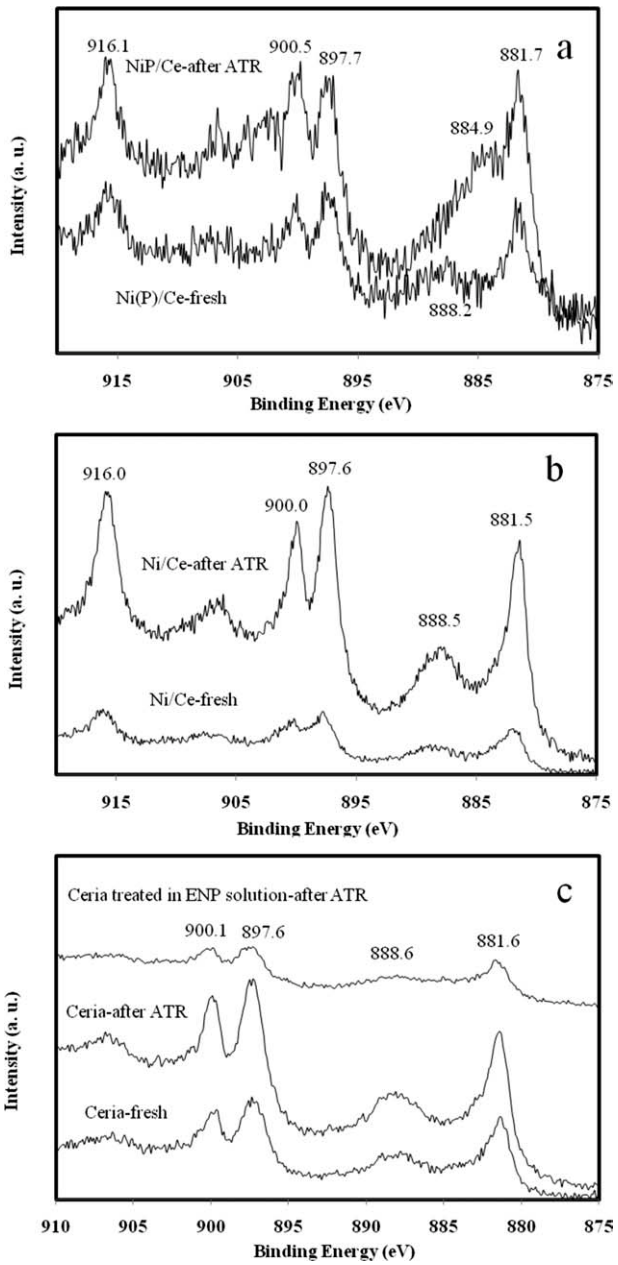

Figure 12. The Ce XPS 3*d* core level spectra of (a) NiP/Ce (b) Ni/Ce catalysts and (c) ceria before and after 8-h ATR of *n*-octane respectively.

other phosphorous compounds. On the contrary, NiP/Ce is a different system, where P forms covalent bond with Ni and hence the P component is unlikely to reduce Ce^{4+} ions, which has been justified by the XPS study. Meanwhile, the control catalyst developed by the blank ENP shows no any phosphorous compound residue as well as Ce^{3+} species. This means that the generation of Ce^{3+} species in the support is not caused by the reduction in the ENP system. It also indicates that Pd is not responsible to the enhanced reducibility of ceria as the preparation of this control catalyst went through the sensitization and activation treatment prior to the test. In the TPR examination of NiP/Ce (Figure 1b), the phenomenon of enhancing reducibility of Ce^{4+} by NiP has been verified. Although the true root cause for why the Ce^{3+} species is generated only in the support on which NiP particles but rather Ni particles are overlaid is still not clear, the presence of NiP phase is surely responsible to the reduction of partial Ce^{4+} ions in ceria to Ce^{3+} ions during ATR. In this context, the NiP phase is presumed to mediate the reduction of surface Ce^{4+} ions by the deposited carbon. The O^{2-} ion conducting $Ce^{III}\ Ce^{IV}_{1-n}\ O_{2-y}$ phase generated could in turn facilitate gasification of the deposited carbon.[31] Consequently, the fact that NiP/Ce catalyst reveals resistance to coke deposition can be attributed to the two complementary factors: a slight increase in charge density at the Ni atoms and the presence of oxygen vacancies in the ceria support. The presence of Ce^{3+} ions in the ceria support of NiP can be also verified by TPO experiment (Figure 10). A rather strong peak happening at about 870°C on the TPO diagram of the used NiP/Ce catalyst reflects oxidation of Ce^{3+} ions.[32]

Finally, it may need to bring up that the Pd colloids used to initiate electroless nickel plating do not contributes to the reforming. Although only a trace amount of Pd in the NiP/Ce (namely less than 0.3 wt % Pd of NiP) could be found by ICP-MS, which was performed by dissolving the sample in a nitric acid solution, none of the Pd species can be detected by XPS on NiP/Ce. This is expected as Pd colloids function as seeds for the growth of Ni-P alloy, hence they are quickly covered up by the Ni(P) alloy soon after plating. As a result, these Pd sites are inaccessible despite being catalytically reactive.

Evaluation of the catalysts in ATR of n-octane containing naphthalene

Fossil fuels usually contain a certain amount of aromatic compounds, which are much more stagnant than alkanes to be reformed and will worsen the coking extent therefore. In this study, we selected naphthalene because it is present in gasoline or diesel for improving octane rating.[33] The feed stream of hydrocarbon was made up of 94 wt % *n*-octane and 6 wt % naphthalene. It has been noted in the preceding discussion that the NiP/Ce and CC catalysts possess better coking resistance than the Ni/Ce catalyst. The inclusion of naphthalene in *n*-octane could thus strengthen the test standard for coking resistance of the NiP/Ce and the CC catalysts.

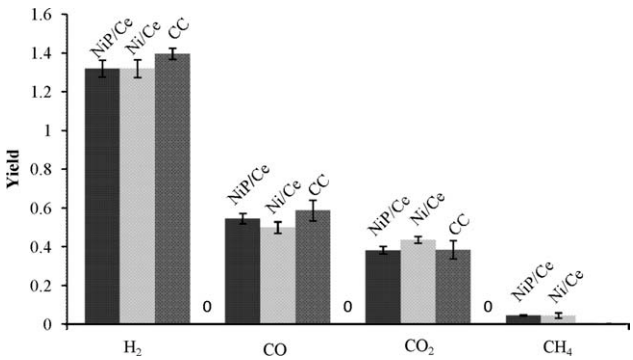

Figure 13. Comparison of the average product yields during 8-h ATR of *n*-octane containing 6 wt % naphthalene in three catalytic systems (C_8H_{18} = 0.04 ml min^{-1}, O_2/C = 0.5, H_2O/C = 1.7, 900°C, GHSV = 9000 ml h^{-1} g_{cat}^{-1}).

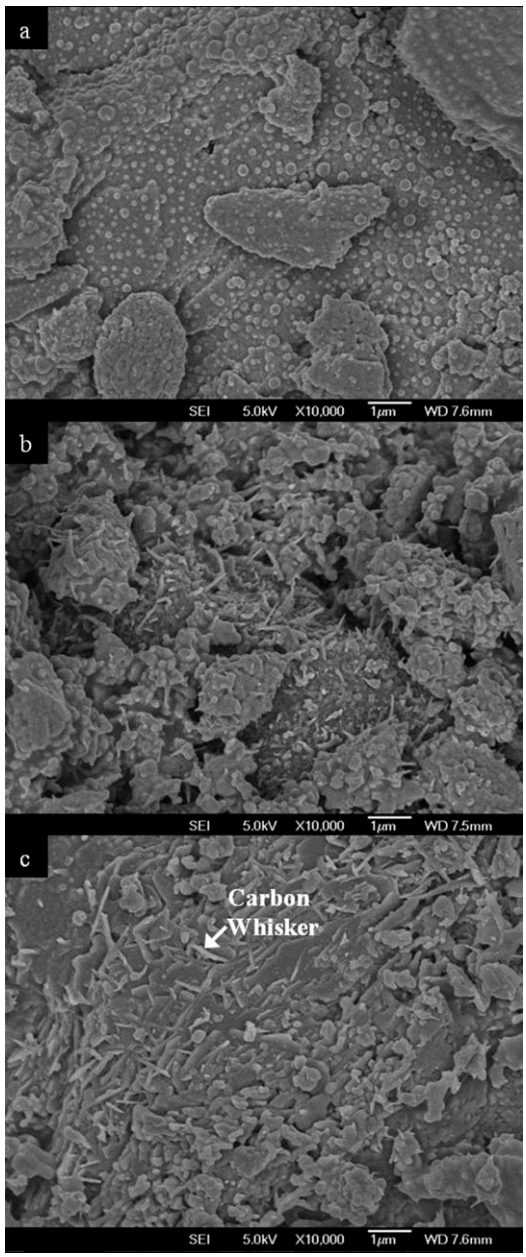

Figure 14. FE-SEM images of (a) NiP/Ce, (b) Ni/Ce, and (c) CC catalysts after 8-h ATR of *n*-octane with 6 wt % naphthalene.

The conversions of the hydrocarbon stream exhibit insignificant difference over the 8 h reaction duration (Table 2). In addition, the yields of the four compounds in the product stream over the 8 h reaction (Figure 13) are slightly different from those presented in Figure 6. The CC catalyst still presents a slightly higher H_2 yield than the NiP/Ce catalyst within this reaction period of time, whereas the Ni/Ce catalyst presents about the same H_2 yield as the NiP/Ce catalyst because the Ni/Ce produces a small amount of CH_4 in this system in contrast to the absence of naphthalene. As estimated, the FE-SEM examination of the spent catalysts (Figure 14) reveals carbon filaments deposition not only on Ni/Ce catalyst but also on the CC catalyst in this case. Clearly, the CC catalyst becomes vulnerable to reform naphthalene. Unlike the two references, the NiP/Ce catalyst still remained free of coking under the same ATR conditions.

The Ni 2*p*, P 2*p*, and Ce 3*d* XPS spectra of NiP/Ce and Ni/Ce catalysts downloaded from this relatively tougher reforming system were examined as well. Similar to the previous finding, an enhancement of electron density at Ni and the occurrence of Ce^{3+} species are also found in the used NiP/Ce catalyst. Especially in the Ce 3*d* spectra, the peak at 885.0 eV for Ce^{3+} is stronger than that in Figure 12; and another strong peak at 903.4 eV which is also characteristic for Ce^{3+} species can be found. In line with the rationale described above, we are inclined to deem that a stronger coking extent due to the presence of naphthalene enhanced reduction of Ce^{4+} ions under the mediation role of the NiP catalytic sites.

Conclusions

The electroless deposition of nickel phosphorus alloy, Ni(P), nodules ($\sim$ 100 nm) on ceria particles of several microns in size is achieved. The ceria-supported Ni(P) is used to catalyze the autothermal reforming (ATR) of *n*-octane and *n*-octane-naphthalene (6 wt %) mixture, respectively. The impregnated Ni/Ce catalyst and a nickel-based commercial SR catalyst (CC) are used as the control catalysts. The ATR is carried out under the conditions comprising O_2/C ratio (=0.5), H_2O/C ratio (=1.7), GHSV = 9000 ml h^{-1} $g_{cat}{}^{-1}$, hydrocarbon = 0.04 ml min^{-1}, and at the reaction temperature of 900°C. The amorphous Ni(P) alloy was converted to the crystalline nickel phosphide Ni_xP_y (x/y $\sim$ 3.7 by mole) in situ under the ATR conditions, which is named as NiP/Ce for simplicity. The XPS analysis shows that there is a slight increase in charge density at the Ni atoms in NiP/Ce compared with that in Ni/Ce. Besides this, the surface of ceria support is changed to an O^{2-}-conducting $Ce^{III}\ Ce^{IV}_{1-n}\ O_{2-y}$ phase by ATR, but it does not happen in the Ni/Ce catalyst. The enhanced reducibility of ceria in NiP/Ce catalyst is supported by the TPR test. Such variations in charge allocation and doping state render the NiP/Ce catalyst resistance against coking, but the two control catalysts are prone to coking, especially in the ATR of the *n*-octane-naphthalene (6 wt %) mixture, over an arbitrarily set reaction duration of 8 h. It is supposed that the NiP nano grains, the catalytic sites, facilitate the reduction of those Ce^{4+} ions located over the surface of support by the deposited coke to form Ce^{3+} ions. Accompanying the formation of Ce^{3+}, the oxygen vacancies are induced in the ceria support.

Acknowledgments

This research work has been supported by the research grant R279000259112 from the faculty of engineering National University of Singapore.

Literature Cited

1. Kang I, Bae J, Bae G. Performance comparison of autothermal reforming for liquid hydrocarbons, gasoline and diesel for fuel cell applications. *J Power Sources*. 2006;163:538–546.
2. Kang I, Bae J. Autothermal reforming study of diesel for fuel cell application. *J Power Sources*. 2006;159:1283–1290.
3. Cheekatamarla PK, Lane AM. Catalytic autothermal reforming of diesel fuel for hydrogen generation in fuel cells: I. Activity tests and sulfur poisoning. *J Power Sources*. 2005;152:256–263.

4. Chen X, Gould BD, Schwank JW. n-Dodecane reforming over monolith-based Ni catalysts: SEM study of axial carbon distribution profile. *Appl Catal A Gen*. 2009;356:137–147.
5. Rostrup-Nielsen JR, Sehested J, J.J. Spivey GWR, Davis BH. *Whisker Carbon Revisited. Studies in Surface Science and Catalysis*. Vol.139, Elsevier; 2001:1–12.
6. Chen X, Tadd AR, Schwank JW. Carbon deposited on Ni/CeZrO isooctane autothermal reforming catalysts. *J Catal*. 2007;251:374–387.
7. Feio LSF, Hori CE, Mattos LV, Zanchet D, Noronha FB, Bueno JMC. Partial oxidation and autothermal reforming of methane on Pd/CeO2-Al2O3 catalysts. *Appl Catal A Gen*. 2008;348:183–192.
8. Soyal-BaltacIoglu F, Aksoylu AE, Onsan ZI. Steam reforming of ethanol over Pt-Ni catalysts. *Catal Today*. 2008;138:183–186.
9. Lakhapatri SL, Abraham MA. Deactivation due to sulfur poisoning and carbon deposition on Rh-Ni/Al2O3 catalyst during steam reforming of sulfur-doped n-hexadecane. *Appl Catal A Gen*. 2009; 364:113–121.
10. Alvarez-Galvan MC, Navarro RM, Rosa F, Briceno Y, Gordillo Alvarez F, Fierro JLG. Performance of La,Ce-modified alumina-supported Pt and Ni catalysts for the oxidative reforming of diesel hydrocarbons. *Int J Hydrogen Energy*. 2008;33:652–663.
11. Xue Q, Gao L, Lu Y. Sulfur-tolerant Pt/Gd2O3-CeO2-Al2O3 catalyst for high efficiency H2 production from autothermal reforming of retail gasoline. *Catal Today*. In Press.
12. Larrondo SA, Kodjaian A, Fabregas I, Zimicz MG, Lamas DG, Walsoe de Reca BE, Amadeo NE. Methane partial oxidation using Ni/Ce0.9Zr0.1O2 catalysts. *Int J Hydrogen Energy*. 2008; 33:3607–3613.
13. Zhu T, Flytzani-Stephanopoulos M. Catalytic partial oxidation of methane to synthesis gas over Ni-CeO2. *Appl Catal A Gen*. 2001; 208:403–417.
14. Escritori JC, Dantas SC, Soares RR, Hori CE. Methane autothermal reforming on nickel-ceria-zirconia based catalysts. *Catal Commun*. 2009;10:1090–1094.
15. Huang T-J, Huang M-C. Effect of Ni content on hydrogen production via steam reforming of methane over Ni/GDC catalysts. *Chem Eng J*. 2008;145:149–153.
16. Liu X, Chen J, Zhang J. Hydrodechlorination of chlorobenzene over silica-supported nickel phosphide catalysts. *Ind Eng Chem Res*. 2008;47:5362–5368.
17. Wang K, Hong L, Liu Z-L. Investigation into the roles of sulfur-containing amino acids in electroless nickel plating bath. *Ind Eng Chem Res*. 2008;47:6517–6524.
18. Cheekatamarla PK, Lane AM. Catalytic autothermal reforming of diesel fuel for hydrogen generation in fuel cells: II. Catalyst poisoning and characterization studies. *J Power Sources*. 2006;154:223–231.
19. Li Y, Wang X, Xie C, Song C. Influence of ceria and nickel addition to alumina-supported Rh catalyst for propane steam reforming at low temperatures. *Appl Catal A Gen*. 2009;357:213–222.
20. Wang K, Hong L, Liu Z-L. Exploring the water-soluble phosphine ligand as the environmentally friendly stabilizer for electroless nickel plating. *Ind Eng Chem Res*. 2009;48:1727–1734.
21. Kar KK, Sathiyamoorthy D. Influence of process parameters for coating of nickel-phosphorous on carbon fibers. *J Mater Process Technol*. 2009;209:3022–3029.
22. Guggilla VS, Akyurtlu J, Akyurtlu A, Blankson I. Steam reforming of n-Dodecane over Ru-Ni-Based catalysts. *Ind Eng Chem Res*. 49:8164–8173.
23. Cecilia JA, Infantes-Molina A, Rodriguez-Castellon E, Jimenez-Lopez A. A novel method for preparing an active nickel phosphide catalyst for HDS of dibenzothiophene. *J Catal*. 2009;263:4–15.
24. Sawhill SJ, Phillips DC, Bussell ME. Thiophene hydrodesulfurization over supported nickel phosphide catalysts. *J Catal*. 2003;215: 208–219.
25. Abu II, Smith KJ. The effect of cobalt addition to bulk MoP and Ni2P catalysts for the hydrodesulfurization of 4,6-dimethyldibenzothiophene. *J Catal*. 2006;241:356–366.
26. Yin X, Hong L, Chen B-H. Role of a Pb2+ stabilizer in the electroless nickel plating system: a theoretical exploration. *J Phys Chem B*. 2004;108:10919–10929.
27. Yu X, Li H, Deng J-F. Selective hydrogenation of adiponitrile over a skeletal Ni-P amorphous catalyst (Raney Ni-P) at 1 atm pressure. *Appl Catal A Gen*. 2000;199:191–198.
28. Sawhill SJ, Layman KA, Van Wyk DR, Engelhard MH, Wang C, Bussell ME. Thiophene hydrodesulfurization over nickel phosphide catalysts: effect of the precursor composition and support. *J Catal*. 2005;231:300–313.
29. Korsvik C, Patil S, Seal S, Self WT. Superoxide dismutase mimetic properties exhibited by vacancy engineered ceria nanoparticles. *Chem Commun*.2007:1056–1058.
30. Xu L, Guo G, Uy D, O'Neil AE, Weber WH, Rokosz MJ, McCabe RW. Cerium phosphate in automotive exhaust catalyst poisoning. *Appl Catal B Environ*. 2004;50:113–125.
31. Song H, Ozkan US. Changing the oxygen mobility in Co/Ceria catalysts by Ca incorporation: implications for ethanol steam reforming. *J Phys Chem A*. 2009;114:3796–3801.
32. Rocchini E, Vicario M, Llorca J, de Leitenburg C, Dolcetti G, Trovarelli A. Reduction and oxygen storage behavior of noble metals supported on silica-doped ceria. *J Catal*. 2002;211:407–421.
33. Kreith F, Goswami Y. *The CRC Handbook of Mechanical Engineering*, 2nd ed. Boca Raton, FL: CRC Press, 2004.

Manuscript received July 7, 2010, revision received Oct. 25, 2010, and final revision received Dec. 6, 2010.